From validation to prediction: Lithospheric field studies from Magsat to *Swarm*

Michael E. Purucker[1], Stefan Maus[2], and Hermann Lühr[3]

[1]*Raytheon ITSS at Geodynamics Branch, GSFC/NASA, USA*

[2]*National Geophysical Data Center, NOAA, USA*

[3]*GeoForschungsZentrum, Potsdam, Germany*

(Received Nov. 15, 2004; Revised xxxx xx, 2004; Accepted xxxx xx, 2004)

Maps of the lithospheric magnetic field made to date have used single satellite observations. In contrast, the upcoming *Swarm* mission will measure the magnetic field gradient, in this case the difference in the magnetic field between the lower two satellites. We discuss our rationale for choosing the satellite separation, and the expected resolution achievable. We relate this gradient to the underlying magnetic field sources, and illustrate its utility with close encounter data from Ørsted and CHAMP. We find that gradient data are superior to field data in isolating the lithospheric signal. We also recognize one or more unmodeled high degree non-lithospheric signals over the oceans. Much current and previous research using satellite magnetic data has focused on signal validation. We are now entering an era in which the satellite data will be used for predictive purposes. For example, the higher resolution will improve our knowledge of isochron location in poorly surveyed parts of the ocean, with significant consequences to our understanding of the tectonics in these regions. The magnetic data can also provide insight into heat flux under ice sheets, for example in the Antarctic and Greenland, and illuminate one of the variables that affect the long-term stability of those ice sheets. When the magnetic data are combined with constraints from other areas of geology and solid earth geophysics, new insights are possible. We illustrate this with an example from the Sunda Arc region of southeast Asia. Between Singapore and the southern end of Borneo, a linear magnetic feature suggests the existence of a now inactive major fault that accomodated much of the strike-slip component from an earlier obliquely convergent plate margin, much as the Great Sumatran Fault does today in a similar plate margin environment. We expect that the higher resolution achievable from *Swarm* will close the spectral gap between current satellite maps and aeromagnetic surveys, and permit a top to bottom view of the crust, and the development of a World Digital Magnetic Anomaly Map.

Key words: gradient, magnetic field, satellite, lithosphere, heat flow, plate tectonics

1. Introduction

Plate tectonics successfully describes the Earth's oceanic lithosphere in terms of rigid body motions of a small numbers of plates, although sparse data coverage hinders even this level of understanding in the southern oceans. Deformation in the continents behaves differently and is not confined to plate boundaries. Current thinking relates the diffuse character of continental deformation to the thickness of its constituent parts. However, the thermal regime, thickness, and deep structure of the lithosphere below continents are still poorly known [*Langel and Hinze*, 1998].

The lithospheric magnetic anomaly field is produced by spatial variations in the magnetisation carried by crustal and some mantle rocks. This magnetisation is partly induced by the ambient field, and is therefore proportional to its strength, the magnetic susceptibility of the rock, and the thickness of the magnetic crust. It can also be a remanent magnetisation acquired during the formation of the rock, which may be reset by thermal or chemical alteration, or by metamorphic phase changes. The magnetic stripes on the sea floor are an example of remanent magnetisation. Until recently, remanent magnetisation in continental crust was thought to have little or no expression in the longer wavelengths of the continental anomaly field measurable from satellite. This paradigm has been shaken with the recent discovery of large-scale remanent magnetisation on the planet Mars, showing intensities an order of magnitude larger than anything seen over the Earth [*Acuña et al.*, 1999; *Langlais et al.*, 2004].

The magnetic field originating from the lithosphere appears globally weaker in the oceanic domain than above continental areas. If this reflects the difference of a factor of five in thickness between continental and oceanic crust, it would suggest that induced magnetisation or viscous remanent magnetisation is likely to be the dominant type of magnetisation in the deeper layers of the crust as well as in the upper mantle. Predominantly associated with the presence of magnetite, the distribution of induced magnetisation depends on gradually changing parameters such as mineralogical composition or in-situ temperature and pressure conditions. The field from the core of the Earth masks the lithospheric field at spherical harmonic degrees up to 13, while degrees 14-18 are a mix of both fields. Hence the

resolvable lithospheric field contains only wavelengths less than 2800 km. Some features in maps of the observed field can be interpreted as edge effects from even longer wavelength fields [*Cohen and Achache*, 1994]. For example, the large East European platform appears as a ring of smaller anomalies in the anomaly map. The resolution of present day satellite data is sufficient to resolve only the widest sea-floor stripes, those associated with the Cretaceous quiet zones, although the satellite data are also capable of resolving the enhanced magnetisation associated with spreading ridges.

Recent satellite data have enhanced our knowledge of the global and regional magnetisation of the crust and uppermost mantle [*Hemant et al.*, 2004], with attendant geodynamic implications. Measurements of the lithospheric field have been used for structural interpretations, for example to show that the European Tornquist-Teisseyre Zone is a first-order feature characteristic of both the upper and lower crust [*Ravat et al.*, 1993], and for delineating the thermo-mechanical properties of the lithosphere, as for example, in the Central America trench.

This paper addresses two topics. First, we demonstrate the enhanced resolution and increased accuracy possible when using the gradient of the magnetic field, as opposed to the field itself. Second, we show with two examples how the magnetic field information can be used for novel tectonic interpretations.

2. Research objectives of *Swarm*

Previous satellite missions have focused on signal validation, in part because the resolution of those missions was insufficient to image the entire crust. There remains a spectral hole between spherical harmonic degrees 60 and 150, corresponding to medium scale features in the lower and middle crust. Degrees higher than 150, corresponding mainly to the upper crust, are accessible from high-quality airborne surveys. The higher resolution provided by the *Swarm* satellites, in combination with more comprehensive approaches to characterizing the field sensed by aeromagnetic surveys, will allow for global compilations of lithospheric fields at scales from 5-3000 km, and provide our first ever, top to

bottom view of the crust.

In the oceans, the increased resolution of the *Swarm* satellites will allow, for the first time, the delineation of oceanic magnetic stripes laid down during times of reversing polarity. This is important because the sparse data coverage in the southern oceans, and poor control of all long-wavelengths, limits our first-order understanding of plate tectonics in the oceanic lithosphere. In addition, two of the three largest ocean basins are dominated by north-south trending magnetic anomaly stripes, and along-track features such as these have proven difficult to extract from a single polar-orbiting satellite. The side-by-side (east-west) separation of the lower two satellites of the *Swarm* constellation is designed to solve this problem [*Olsen et al.*, 2004].

3. Gradients and close encounter data from Ørsted and CHAMP

To improve the resolution of lithospheric magnetisation mapping, the satellites will fly at low altitudes. The selected altitude ranges will, however, be compatible with a multi-year mission lifetime. Further improvement in the retrieval of the high-degree magnetic anomalies field can be achieved by considering gradients in the inversion algorithm, in addition to the full magnetic field readings. This concept for emphasising the small-scale anomalies by partially counteracting the attenuation effect with altitude has already been accepted and applied in gravity missions like GRACE and GOCE [*ESA*, 1999]. Optimal spacecraft separations for deriving the gradients are dependent on signal spectrum and instrument resolution. An additional consideration is the definition of the smallest scales that should be resolved during the mission. The spacecraft separation should be large enough to provide an easily measurable gradient signal.

In order to find the optimal longitudinal separation of the lower pair of satellites for crustal field studies, we consider the following scenario: The scalar potential describing the crustal field $\mathbf{B}_{\rm cr} = -\mathrm{Re}\{\mathrm{grad}\, V\}$, is given as a spherical harmonic expansion,

$$V_{\rm cr} = a \sum_{n=1}^{n_{\max}} \sum_{m=0} \left(\frac{a}{r}\right)^{n+1} \gamma_n^m P_n^m e^{im\phi}.$$

This is the complex form of the usual spherical harmonic summation used in geomagnetism, with $\gamma_n^m = g_n^m - ih_n^m$.

The difference of the magnetic field measured by two satellites flying simultaneously with a longitudinal separation $\Delta\phi$ is $\Delta\mathbf{B}_{\rm cr} = \mathbf{B}_{\rm cr}(r,\theta,\phi) - \mathbf{B}_{\rm cr}(r,\theta,\phi+\Delta\phi) = -{\rm Re}\{{\rm grad}\ \Delta V\}$, where ΔV is a spherical harmonic expansion with coefficients $\Delta\gamma_n^m = \gamma_n^m\left(1 - e^{im\Delta\phi}\right)$. Hence by analysing the difference of the magnetic field measured by the two satellites the crustal field coefficients γ_n^m are multiplied with some filter factors, and the filter gain is $|\left(1 - e^{im\Delta\phi}\right)| = \sqrt{2(1-\cos m\Delta\phi)}$.

Figure 1 shows the filter gain for three different values of longitudinal separation, $\Delta\phi$, of the satellites. Since *Swarm* aims at the determination of the lithospheric field up to spherical harmonic degree and order 133 (spatial scale of 300 km), the optimal longitudinal separation of the lower satellites is about 1.4°.

A further advantage is that signals from large-scale external contributions that predominantly change in north-south direction are suppressed by the gradient method applied in the east-west direction [*Olsen et al.*, 2004]. Another advantage of using the East-West gradient as opposed to the originally proposed pair of following spacecraft [*Friis-Christensen et al.*, 2002] is that for short time intervals (approximately within 10 seconds), gradients along both neighbouring tracks can still be used.

The magnitude, and pattern, of the east-west gradient of a model total field anomaly map, ΔF can be seen in Figure 2. The total field anomaly F at point $\mathbf{r}$, is related to the vector magnetic field $\mathbf{B}$ through $F = \hat{\mathbf{b}} \cdot \mathbf{B}$, where $\hat{\mathbf{b}}$ is the unit vector of the ambient field at $\mathbf{r}(r,\theta,\phi)$.

This model is developed on a $0.5^\circ \times 0.5^\circ$ grid of vertically integrated remanent magnetization developed by [*Dyment and Arkani-Hamed*, 1998b] for the oceanic crust. The model is based on an age map of the oceans, the relative motion of the plates, and the African Apparent Polar Wander Path. No magnetic field observations were used in producing the original model, but it has subsequently been calibrated against observations of the satellite anomaly field in the North and South Atlantic [*Purucker and Dyment*, 2000]. Note that there are five minimums in the gradient map along its southern

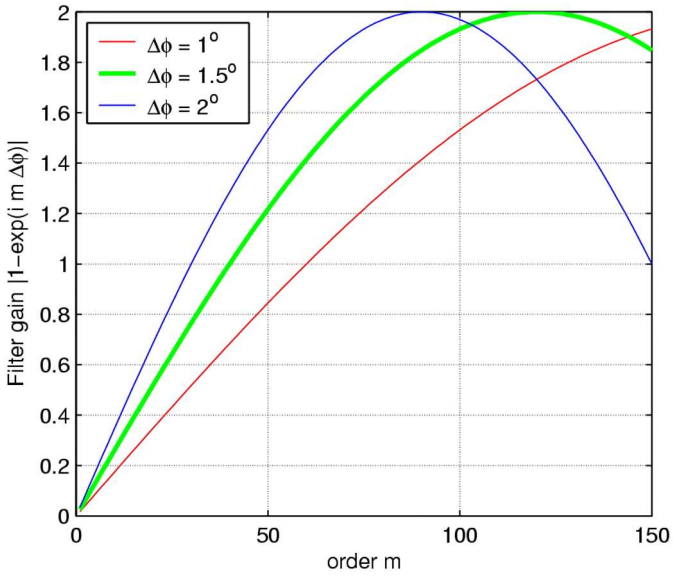

Fig. 1. Relative sensitivity of the gradient method versus spatial scales (spherical harmonic order m). Three examples with different spacecraft separations in longitude are shown.

boundary, as compared to only three minimums in the total field map. This enhanced resolution is accompanied by a decrease in signal magnitude by about a factor of two relative to the total field map. We expect, however, that these gradients should be easily measurable with both our total field and vector instruments. Additional, and complementary, gradient information will be available from the vector magnetic field gradients. This additional information should be especially helpful in deconvolving the lithospheric field signature near the geomagnetic equator, in addition to its use in characterizing external fields.

It is useful to be able to express the measured gradient ΔF in terms of a source function like equivalent source dipoles [*Mayhew*, 1979] for two reasons. First, it allows us to reduce data collected at different altitudes to a common altitude. Second, it provides some insight into the lateral variation of magnetization. The magnetic field $\mathbf{B}(\mathbf{r})$ at a location $\mathbf{r}(r, \theta, \phi)$ caused by a magnetic point dipole $\mathbf{M}(M_{r_1}, M_{\theta_1}, M_{\phi_1})$ at a location $\mathbf{r_1}(r_1, \theta_1, \phi_1)$ can be shown [*Dyment and Arkani-Hamed*, 1998a; *Von Frese et al.*, 1998] to be

where δ is the angle between $\mathbf{r}$ and $\mathbf{r_1}$ and the other symbols are defined as

Then $\Delta F = ((\hat{\mathbf{b}_\mathbf{a}} \cdot \mathbf{B_a}) - (\hat{\mathbf{b}_\mathbf{b}} \cdot \mathbf{B_b}))/R_{ab}$, where the a subscript indicates a measurement by the first

$$
\begin{aligned}
\mathrm{B}_r &= \tfrac{-1}{R^3}\left[\left(\tfrac{3AA_1}{R^2}+\cos\delta\right)\mathrm{M}_{r_1}+\left(\tfrac{3AB_1}{R^2}-\tfrac{B_1}{r}\right)\mathrm{M}_{\theta_1}\right.\\
&\qquad\left.+\left(\tfrac{3AC_1}{R^2}-\tfrac{C_1}{r}\right)\mathrm{M}_{\phi_1}\right],\\
\mathrm{B}_\theta &= \tfrac{-1}{R^3}\left[\left(\tfrac{3BA_1}{R^2}-\tfrac{B}{r_1}\right)\mathrm{M}_{r_1}+\left(\tfrac{3BB_1}{R^2}+D\right)\mathrm{M}_{\theta_1}\right.\\
&\qquad\left.+\left(\tfrac{3BC_1}{R^2}+E\right)\mathrm{M}_{\phi_1}\right],\\
\mathrm{B}_\phi &= \tfrac{-1}{R^3}\left[\left(\tfrac{3CA_1}{R^2}-\tfrac{C}{r_1}\right)\mathrm{M}_{r_1}+\left(\tfrac{3CB_1}{R^2}-F\right)\mathrm{M}_{\theta_1}\right.\\
&\qquad\left.+\left(\tfrac{3CC_1}{R^2}+G\right)\mathrm{M}_{\phi_1}\right],
\end{aligned}
$$

$$
\begin{aligned}
R &= (r^2+r_1^2-2rr_1\cos\delta)^{1/2},\\
\cos\delta &= \cos\theta\cos\theta_1+\sin\theta\sin\theta_1\cos(\phi-\phi_1),\\
A &= r-r_1\cos\delta,\\
B &= r_1\left(\sin\theta\cos\theta_1-\cos\theta\sin\theta_1\cos(\phi-\phi_1)\right),\\
C &= r_1\sin\theta_1\sin(\phi-\phi_1)\\
D &= \sin\theta\sin\theta_1+\cos\theta\cos\theta_1\cos(\phi-\phi_1),\\
E &= \cos\theta\sin(\phi-\phi_1),\\
F &= \cos\theta_1\sin(\phi-\phi_1),\\
\mathrm{G} &= \cos(\phi-\phi_1).\\
A_1 &= r_1-r\cos\delta,\\
B_1 &= r\left(\cos\theta\sin\theta_1-\sin\theta\cos\theta_1\cos(\phi-\phi_1)\right)\\
\text{and } \mathrm{C}_1 &= -r\sin\theta\sin(\phi-\phi_1).
\end{aligned}
$$

satellite, a b subscript one by the second satellite and R_{ab} is the distance between the two satellites.

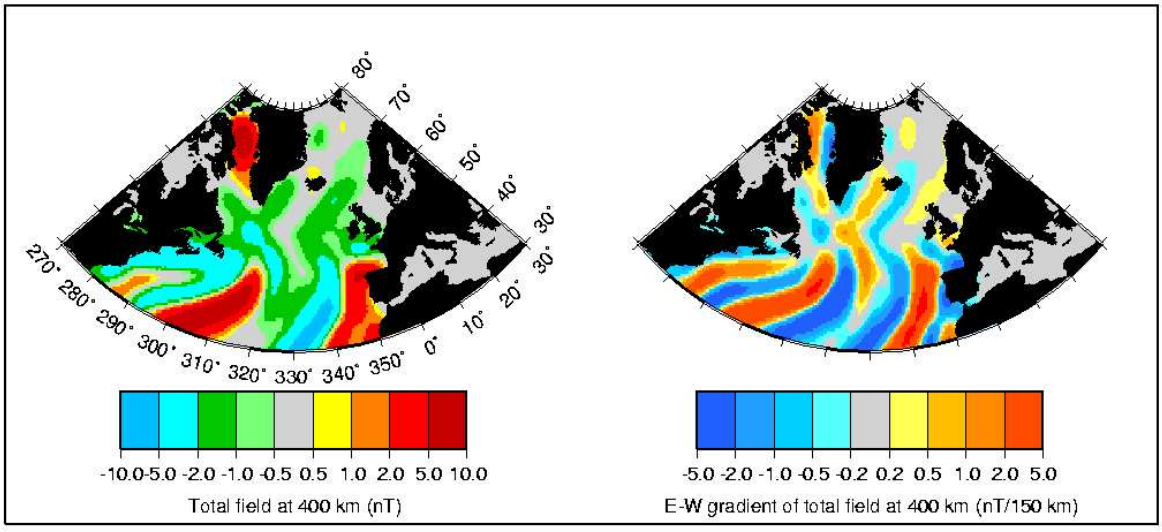

Fig. 2. A comparison of a map of the E-W gradient of the total field with the total field map for the same area. A separation of 1.5° is used in the E-W gradient calculation.

We can demonstrate the superiority of a gradient measurement to a field measurement with an

example from close encounters of the Ørsted and CHAMP satellites. Figure 3 includes the locations of all close encounters of these two satellites from shortly after the launch of CHAMP (2000) to the spring of 2004. We have selected close encounters that mimic to a significant degree the conditions to be expected in the *Swarm* constellation. We have limited the close encounters to those in which the sub-satellite points were within 1.5° of one another. We did not have to specify a minimum distance because the altitude of the spacecraft differ by 300 km, ensuring the presence of an adequate gradient. No selection was made on the basis of magnetic activity level or local time, as is normally done. This was done to illustrate the fact that gradient measurements are much less sensitive to those parameters than are field measurements, except in the case where the satellite is passing through regions, like the northern and southern auroral ovals, where the spatial variability of the field is comparable to the spacecraft separations. The figure clearly demonstrates that gradient data are superior to field data in isolating the lithospheric signal. We also recognize in this figure the presence of one or more unmodeled high degree non-lithospheric signals over the oceans.

4. Crustal thickness and heat flux estimates from magnetic field measurements

In order to minimize time-variable fields associated with the interaction of the solar and terrestrial dynamos, we usually utilize spherical harmonic models built from data gathered during magnetically quiet times, rather than the field data directly. Both CM4 [*Sabaka et al.*, 2004], and MF-3 [*Maus et al.*, 2005] are models of this type, and have been used by us for lithospheric field studies. The two models reflect somewhat different design philosophies, and hence have different strengths. MF-3 is a lithosheric field model only, and extends from degree 16 to 90. The CHAMP magnetic field satellite input to MF-3 has had removed an internal field model to degree 15, an external field model of degree 2, and the predicted signatures from eight main ocean tidal components. Additional external fields are subsequently removed in a track-by-track scheme. Because of its design philosophy, the MF-3 estimate can be considered a minimum estimate of the lithospheric magnetic field, one in which there will

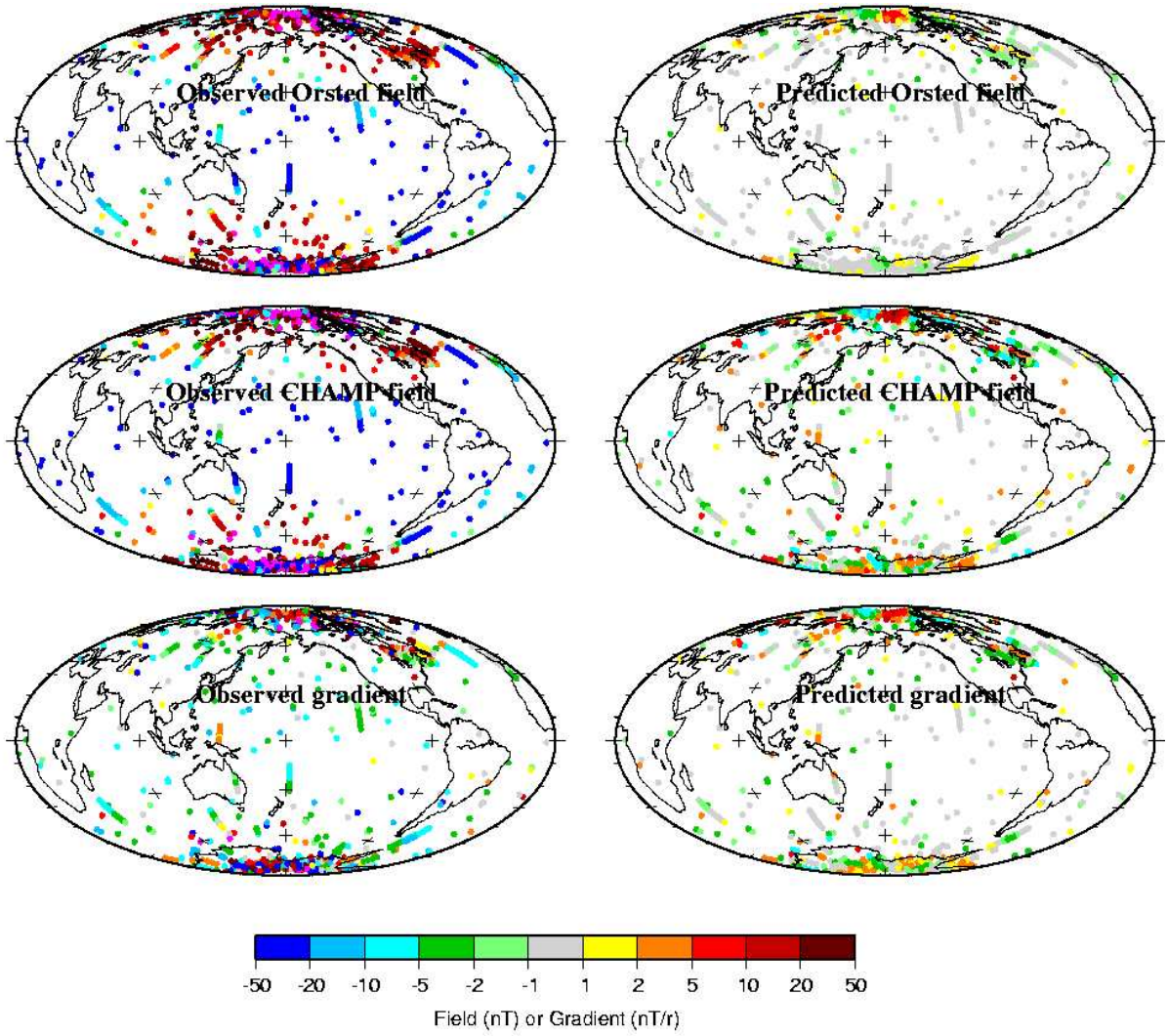

Fig. 3. Total field (top and middle rows) and total field gradient (bottom rows) during close encounters of Ørsted and CHAMP (2001-2004). The circles locate observation points where the two satellites had sub-satellite locations within 1.5° of one another at the same instant in time. The circles are color coded with the field or gradient information. The two satellites are separated by about 300 km in altitude, with CHAMP being lower. The observed fields (left row) are shown after removal of CM-4 based models of the main, ionospheric, and magnetospheric fields. The predicted fields (right row) are static degrees 14-65 from that same magnetic field model. That same magnetic (main+external) field model is removed prior to calculation of the observed gradient.

be some suppression of along-track magnetic fields. Regularization has been applied to degrees higher than 60 to extract clusters of spherical harmonic coefficients that are well-resolved by the data. CM4, in contrast, is a comprehensive model, and includes components of internal and external origin, in addition to toroidal fields. It includes data from all high-precision magnetic field missions back to the 1960's. It uses an iteratively reweighted least squares approach to solve for all of the 25000+ parameters using

more than 2 million observations. Because of its design philosophy, the CM4 estimate is expected to have more power than MF-3, both because no direct damping is applied to the lithospheric field coefficients, and because of the along-track approach used by MF-3. No suppression of along-track magnetic fields is expected, and some of them, especially in the vicinity of the dip equator, are of questionable lithospheric origin.

The magnetic crustal thickness is derived using an iterative approach. We first remove a model of the remanent magnetism in the oceanic crust [*Dyment and Arkani-Hamed*, 1998b; *Purucker and Dyment*, 2000]. We have no comparable model for remanent magnetism in the continental crust, so we will assume that remanent magnetism in continental crust is absent. This will lead to an over-estimation of magnetic crustal thickness over features dominated by remanent magnetism, probably including the Kursk and Bangui anomalies. Contributions from spherical harmonic degrees less than 15 are also discarded from the remanent magnetic model, to avoid the low degree spectral band of inseparable crustal and core fields. Because of this separation problem, we need to introduce an initial model for the magnetic crustal thickness. We choose as our initial model the 3SMAC seismic tomographic model [*Nataf and Ricard*, 1996], which describes, in a self-consistent manner, a host of physical attributes, including thermal properties and thicknesses of the constituent parts of the lithosphere. We assume a low-Ti magnetite as the dominant magnetic carrier in the deep crust. Other initial models, such as ones derived from Crust 5.1 [*Mooney et al.*, 1998; *Bassim et al.*, 2000] can be expected to result in slightly different magnetic crustal thicknesses. From this initial model, we calculate the predicted induced field using the equivalent source formalism discussed earlier. We use a simple susceptibility model that assumes a single constant value for continental (0.035 SI) and oceanic (0.04 SI) crust, which carries with it the assumption that lateral variations in magnetic susceptibility are subordinate to magnetic crustal thickness variations. We justify this assumption because the predicted and observed magnetic fields have many similarities. Next, the predicted magnetic field is subtracted from the observed magnetic field, and this difference map is inverted to yield a magnetic thickness correction. This magnetic

thickness correction is added to the original magnetic thickness model, and a new field is calculated. Subsequent to the application of the high-pass filter, this field is again compared to the magnetic field observations. This procedure continues until the process converges, and the observation and prediction are within some RMS error. This is typically about 0.5 nT.

To estimate the geothermal heat flux [*Fox Maule et al.*, 2004], a 1-D heat conduction model is used, with constant thermal conductivity. Heat production by crustal sources is assumed to decrease exponentially with depth, and to be laterally uniform. The presence of discrete granitic bodies within the crust will violate this assumption, but we consider that the height of the satellite limits our resolution to 400+ km laterally, and so we expect that single granitic bodies will not be visible from satellite. The heat flux map will, as a consequence, reflect the variation in magnetic crustal thickness. We also recognize that these assumptions are only appropriate for continental crust.

5. Examples

5.1 Isochron location in the southern Pacific

The higher resolution of *Swarm* will improve our knowledge of isochron location in poorly surveyed parts of the ocean, with significant consequences to our understanding of the tectonics in these regions. Figure 4 illustrates the current limits to our ability to locate a major isochron, the end of the Cretaceous Quiet zone, in the southeastern Pacific Ocean [*Purucker et al.*, 2003]. The map on the left represents the predicted magnetic fields from a combination of the *Dyment and Arkani-Hamed [1998b]* model over the oceans to describe remanent magnetization and the 3SMAC [*Nataf and Ricard*, 1996] model of induced magnetization. The black lines are the fracture zones, the red lines are seafloor spreading isochrons. The anomalies marked 'B', 'C', and 'D' define the end of the Cretaceous quiet zone here. The map on the right represents the radial magnetic field observations from the CM4 [*Sabaka et al.*, 2004] model. Note that the edge of the Cretacous quiet zone (anomalies 'B', 'C', and 'D' on the observed map) are offset from their predicted location. In the case of 'B', this offset amounts to some

700 km.

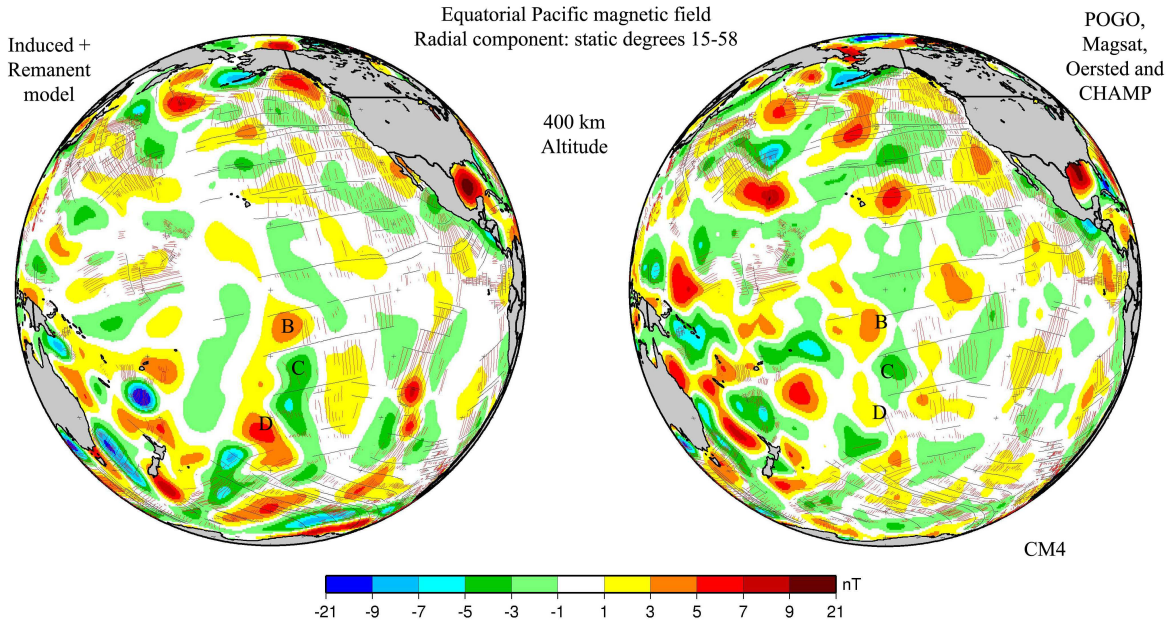

Fig. 4. A revised determination of the southeast edge of the Cretaceous Quiet Zone in the southern Pacific.

5.2 Estimates of heat flux in Australia

Once an estimate of magnetic crustal thickness has been made, it can also provide insight into heat flux, as previously indicated. But before we utilize these heat flux estimates, we would like to validate them using other lines of evidence. For example, *Fox Maule et al. [2004]* find that areas of high heat flux in the Antarctic are preferentially located in areas of current volcanism. In Australia, we can compare our estimates of heat flux (Figure 5, left) with estimates [*Drummond et al.*, 1989] based on teleseismic travel times (Figure 5, middle) and heat flow [*Sass and Lachenbruch*, 1979] provinces (Figure 5, right). Such comparisons give us confidence in the viability of this technique and can provide an estimate of the resolution and limitation of each technique. c

5.3 Singapore-Borneo megashear

As a final example of the predictive capability of the current generation of magnetic field models, we examine the MF-3 magnetic model over the Sunda Arc region of southeast Asia (Figure 6). The

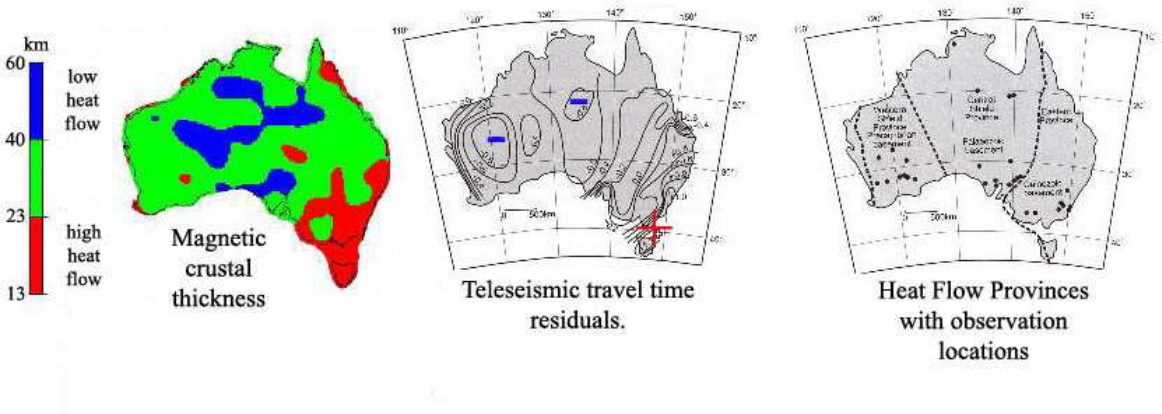

Fig. 5. Magnetic crustal thickness and heat flux in Australia determined using satellite data (left, this study), and comparison with seismically determined heat flux indicators (middle). Positive (red +) teleseismic time residuals are indicative of high heat flow, and negative (blue -) residuals are indicative of low heat flow [*Drummond et al.*, 1989]. Shown at the right are the approximate boundaries of the three major Australian heat flow/age provinces [*Sass and Lachenbruch*, 1979] along with the locations at which heat flow-heat production measurements have been made. The highest heat flows are found in the youngest, Eastern province, intermediate heat flows are found in the central province, and the lowest heat flows are found in the old Western Shield.

magnetic crustal thickness (Figure 6, right) has been prepared as previously described, using as a starting point the 3SMAC model (Figure 6, middle), and refining it with MF-3 (Figure 6, left). Notice that the magnetic data defines an arcuate region of thicker magnetic crust along the Sumatran volcanic island arc. This thickened crust represents the sum of the crust from the island arc, and the underlying subducting slab where its temperature is less than the Curie point. A region of thinned magnetic crust can be seen north of the island arcs, extending as far NW as Singapore (S). Between Singapore and the southern end of Borneo, a linear magnetic feature (from the southern tips of S to B) is evident. This linear magnetic feature seems to be a continuation of the linear coastline NW of Singapore, and suggests a tectonic control. Today, the Great Sumatran Fault (GSF) runs the length of Sumatra, and is located close to a major crustal thickness boundary. GSF accomodates much of the strike-slip component of the current obliquely convergent plate margin in a series of staggered en-echelon faults with bounding step-over basins. Although not well known [*Hamilton*, 1979; *Simoes et al.*, 2004], the earlier history of this plate margin is probably buried beneath arc sediments and volcanics to the north of the current trench. Therefore the linear magnetic feature that we see would be consistent with the

existence of a now inactive major fault that accomodated much of the strike-slip component from an earlier obliquely convergent plate margin, much as the Great Sumatran Fault does today in a similar plate margin environment. We term this linear feature the Singapore-Borneo Megashear.

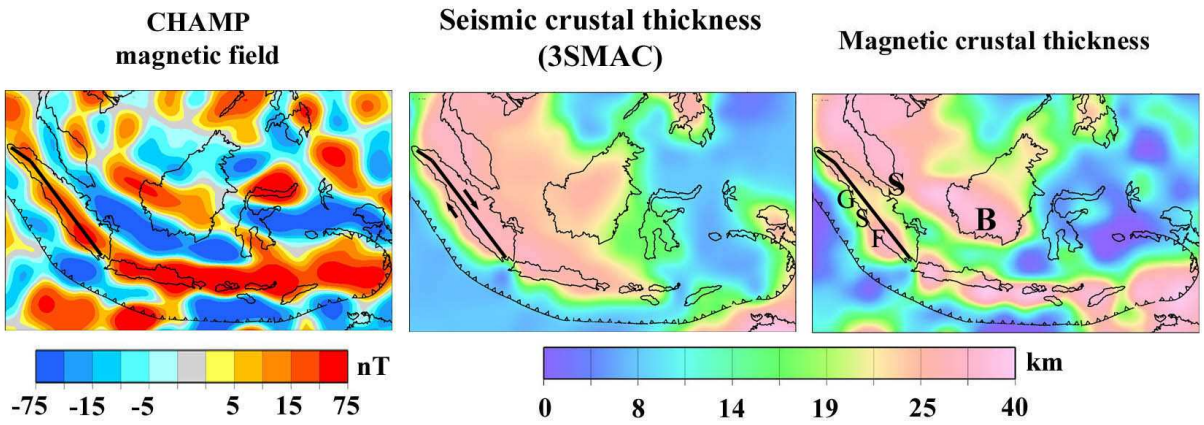

Fig. 6. Radial magnetic field of lithospheric origin to degree 90 (left) and magnetic crustal thickness (right) in the Java trench region. It is based on the joint inversion of magnetic (CHAMP, MF-3) and seismic/thermal (3SMAC) models (centre), with long-wavelength control from 3SMAC and short wavelength control from MF-3. GSF indicates the location of the Great Sumatran Fault, whose offset is shown in the middle panel. The surface expression of the Java trench is shown by the barbed line, with the barbs on the downthrown side. The sharp linear crustal thickness boundary extending from Singapore (S) to the southern boundary of Borneo (B) locates the end points of the proposed Singapore-Borneo Megashear.

6. Conclusion

We expect that the higher lithospheric field resolution achievable from *Swarm* gradient data will close the spectral gap between current satellite maps and aeromagnetic surveys, permit a top to bottom view of the crust, and aid in the development of a World Digital Magnetic Anomaly Map.

Acknowledgments. We thank the Ørsted and CHAMP data centers and project teams for their support. Cathrine Fox Maule, Nils Olsen, and Richard Smith are acknowledged for collaborations on many of the developments discussed here. This effort is part of NASA and GFZ contributions to the ESA-led *Swarm* project. We wish to acknowledge the encouragement of Roger Haagmans and John LaBrecque. MEP is supported under NASA contract NAS5-00181.

7. References

Acuña, M., et al., Global distribution of crustal magnetization discovered by the Mars Global Surveyor MAG/ER experiment, *Science*, *284*, 790–793, 1999.

Bassim, C., G. Laske, and G. Masters, The current limits of resolution for surface wave tomography in North America, *EOS Trans AGU*, *81*, F897, 2000.

Cohen, Y., and J. Achache, Contribution of induced and remanent magnetization to long-wavelength oceanic magnetic anomalies, *J. Geophys. Res.*, *99*, 2943–2954, 1994.

Drummond, B., K. Muirhead, C. Wright, and P. Wellman, A teleseismic travel time residual map of the Australian continent, *BMR Journal of Australian Geology and Geophysics*, *11*, 101–105, 1989.

Dyment, J., and J. Arkani-Hamed, Equivalent source dipoles revisited, *Geophys. Res. Lett.*, *25*, 2003–2006, 1998a.

Dyment, J., and J. Arkani-Hamed, Contribution of lithospheric remanent magnetization to satellite magnetic anomalies over the world's oceans, *J. Geophys. Res.*, *103*, 15,423–15,442, 1998b.

ESA, Gravity Field and Steady-State Ocean Circulation Mission: Report for mission selection, *ESA SP-1233(1)*, ESA Publications Division, ESTEC, Noordwijk, The Netherlands, 1999.

Fox Maule, C., M. Purucker, N. Olsen, and K. Mosegaard, Heat flux anomalies in Antarctica discovered from satellite magnetic data, *Science, submitted*, 2004.

Friis-Christensen, E., H. Lühr, and G. Hulot, *Swarm* - a constellation to study the dynamics of the Earth's magnetic field and its interactions with the Earth system, *DSRI Report 1/2002*, Danish Space Research Institute, Copenhagen, 2002.

Hamilton, W., Tectonics of the Indonesian region, in *U.S. Geological Survey Professional Paper 1078*, U.S. Government Printing Office, 1979.

Hemant, K., S. Maus, and V. Haak, Interpretation of CHAMP crustal field anomaly maps using a geographical information system (GIS) technique, in *Earth Observation with CHAMP, results from Three Years in Orbit*, edited by C. Reigber, H. Luehr, P. Schwintzer, and J. Wickert, pp. 249–254, Springer, Berlin-Heidelberg, 2004.

Langel, R. A., and W. J. Hinze, *The magnetic field of the Earth's lithosphere: The satellite perspective*, Cambridge University Press, 1998.

Langlais, B., M. Purucker, and M. Mandea, Crustal magnetic field of Mars, *J. Geophys. Res.*, *109*, E02,008, doi:10.1029/2003JE002,048, 2004.

Maus, S., M. Rother, K. Hemant, H. Lühr, A. Kuvshinov, and N. Olsen, Earth's crustal magnetic field determined to spherical harmonic degree 90 from champ satellite measurements, *Geophys. J. Int., submitted*, 2005.

Mayhew, M., Inversion of satellite magnetic anomaly data, *J. Geophys.*, *45*, 119–128, 1979.

Mooney, W., G. Laske, and G. Masters, Crust5.1: A global crustal model at $5^\circ \times 5^\circ$, *J. Geophys. Res.*, *103*, 727–747, 1998.

Nataf, H., and Y. Ricard, 3SMAC: an a priori tomographic model of the upper mantle based on geophysical modeling, *Physics of the Earth and Planetary Interiors*, *95*, 101–122, 1996.

Olsen, N., et al., *Swarm* - End-to-End mission performance simulator study, ESA contract No 17263/03/NL/CB, *DSRI Report 1/2004*, Danish Space Research Institute, Copenhagen, 2004.

Purucker, M., T. Sabaka, N. Olsen, and S. Maus, How have Ørsted, CHAMP, and SAC-C improved our knowledge of the oceanic regions?, in *Proceedings of the 4th OIST conference*, edited by Stauning, P. et al., Copenhagen, Denmark, 2003.

Purucker, M. E., and J. Dyment, Satellite magnetic anomalies related to seafloor spreading in the

South Atlantic Ocean, *Geophys. Res. Lett.*, *27*, 2765–2767, 2000.

Ravat, D., H. W.J., and P. Taylor, European tectonic features observed by Magsat, *Tectonophysics*, *220*, 157–173, 1993.

Sabaka, T. J., N. Olsen, and M. Purucker, Extending comprehensive models of the Earth's magnetic field with Ørsted and CHAMP data, *Geophys. J. Int.*, *159*, 521–547, doi: 10.1111/j.1365–246X.2004.02,421.x, 2004.

Sass, J., and A. Lachenbruch, The thermal regime of the Australian continental crust, in *The Earth - Its origin, structure and evolution*, edited by M. McElhinny, pp. 301–352, Academic Press, 1979.

Simoes, M., J. Avouac, R. Cattin, and P. Henry, The Sumatra subduction zone: A case for a locked fault zone extending into the mantle, *J. Geophys. Res.*, *109, B10402, doi:10:1029/2003JB002958*, 2004.

Von Frese, R., W. Hinze, and L. Braile, Correction to "spherical earth gravity and magnetic anomaly analysis by equivalent point source inversion", *Earth and Plan. Sci. Lett.*, *163*, 409–411, 1998.

Michael.Purucker (e-mail: purucker@geomag.gsfc.nasa.gov)